

# The anatomy of Boris type solvers and large time-step plasma simulations

Siu A. Chin\* and Durward Cator

*Department of Physics and Astronomy,*

*Texas A&M University, College Station, TX 77843, USA*

## Abstract

This work gives a Lie operator derivation of various Boris solvers via a detailed study of first and second-order trajectory errors in a constant magnetic field. These errors in the gyro-circle center and gyro-radius are the foundational basis for why Boris solvers existed, independent of any finite-difference schemes. The elimination of these errors then forces the second-order solver's trajectory to be exactly on the gyro-circle. By revisiting some historical calculations, it is found that many publications do not distinguish the poorly behaved first-order leap-frog solver with the correct second-order Boris algorithm. This work shows that this second-order Boris solver is much more accurate than previously thought and that its trajectory remains close to the exact orbit in a combined *nonuniform* electric and magnetic field at time-steps greater than the cyclotron period.

**Key words:** Plasmas simulation, Boris solvers, magnetic field integrators, large time-step methods

\* Corresponding author, chin@physics.tamu.edu

## I. INTRODUCTION

The leap-frog (LF) Boris solver[1, 2] has been widely used in plasma physics simulations[3–12] for decades. However, the original derivation of the Boris solver from the implicit mid-point scheme[1, 2] may not be the most transparent perspective for understanding the inner workings of the Boris solver. For example, the recent derivation of *two* fundamental Boris solvers[13] has shown that the Cayley[9, 14](Crank-Nicolson[12]) form of the rotation matrix is a mere consequence of forcing the magnetic trajectory to be on the gyro-circle, not its cause. In this work, we will derive Boris-type solvers from the Lie operator formalism[15], so that their trajectory errors can be directly determined independent of any finite-difference schemes. In particular, we will examine the large time step behavior of various Boris solvers by revisiting some historical calculations and show that in many cases, the correct Boris solver has not been used.

Leap-frog type algorithms, which update the position and momentum variables sequentially, were historically novel as compared to Runge-Kutta type algorithms, which update variables synchronously. However, the rise of modern symplectic integrators[16–19] (SI), which identified[20] sequential updating as the distinguishing hallmark of canonical transformations, has made sequential updating the new norm for classical dynamics algorithms. While Runge-Kutta schemes are generally not phase-volume preserving, as will be shown in the next Section, *any* sequential updating of the momentum and position variables is automatically volume preserving. Given an initial pair of position and momentum, a LF algorithm will generate a sequence of positions and momenta identical to a first-order SI. For LF, each pair of position and momentum are labeled as half a time-step apart. For SI, each successive pair are regarded as at the same time step. Thus LF algorithms are structurally identical to first-order SI, unless the initial position and momentum were actually specified at half a time-step apart, which is normally not the case. As will be shown in Sect.III and IV, LF Boris solvers have glaringly large first order errors that are immediately recognizable in some published calculations.

We begin by reviewing the less familiar Lie operator method[16–19] of deriving magnetic[15] integrators in Sect.II. The same method is used to derive symplectic integrators, except that by using the mechanical momentum in the Lorentz force law rather than the canonical momentum in the Hamiltonian, the resulting algorithms are Poisson[14] integrators, rather

than symplectic. In Sect.III, we derive two fundamental first-order magnetic field algorithms and scrutinize their trajectory errors for a constant magnetic field. Two distinct choices of eliminating these errors result in two different types of Boris solvers. In Sect.IV, on-orbit second-order Boris solvers are derived, including one that is not derivable from finite-difference schemes. In Sect.V, we show that the inclusion of the electric field in Boris'  $\mathbf{E}$ ,  $\mathbf{B}$  splitting method can be viewed as a consequence of Buneman's original  $\mathbf{E} \times \mathbf{B}$  formulation, but only for the original Boris angle. The second-order Boris solver is shown to be uniquely accurate even at time steps greater than the cyclotron period. Conclusions are summarized in Sect.VI.

## II. THE LIE OPERATOR METHOD

The equations of motion for a charged particle in a static electric  $\mathbf{E}(\mathbf{r})$  and magnetic field  $\mathbf{B}(\mathbf{r}) = B(\mathbf{r})\hat{\mathbf{B}}(\mathbf{r})$  can be written as

$$\frac{d\mathbf{r}}{dt} = \mathbf{v} \quad \text{and} \quad \frac{d\mathbf{v}}{dt} = \omega(\mathbf{r})\hat{\mathbf{B}}(\mathbf{r}) \times \mathbf{v} + \mathbf{a}(\mathbf{r}) \quad (2.1)$$

where  $\mathbf{v} \equiv \mathbf{p}/m$ ,  $\omega(\mathbf{r}) = (-q)B(\mathbf{r})/m$  and  $\mathbf{a}(\mathbf{r}) = \mathbf{F}(\mathbf{r})/m = q\mathbf{E}(\mathbf{r})/m$ . The vectors  $\mathbf{r}$  and  $\mathbf{v}$  are fundamental and independent dynamical variables.

For any other dynamical variable  $W(\mathbf{r}, \mathbf{v})$ , its evolution through (2.1), is given by

$$\begin{aligned} \frac{dW}{dt} &= \frac{\partial W}{\partial \mathbf{r}} \cdot \frac{d\mathbf{r}}{dt} + \frac{\partial W}{\partial \mathbf{v}} \cdot \frac{d\mathbf{v}}{dt} \\ &= \left( \mathbf{v} \cdot \frac{\partial}{\partial \mathbf{r}} + (\omega\hat{\mathbf{B}} \times \mathbf{v} + \mathbf{a}) \cdot \frac{\partial}{\partial \mathbf{v}} \right) W, \end{aligned} \quad (2.2)$$

which can be directly integrated to yield the operator solution

$$W(t) = e^{t(T+V_{BF})}W(0) \quad (2.3)$$

where one has defined Lie operators[16–18]

$$T = \mathbf{v} \cdot \frac{\partial}{\partial \mathbf{r}} \quad (2.4)$$

and

$$V_{BF} = \omega(\hat{\mathbf{B}} \times \mathbf{v}) \cdot \frac{\partial}{\partial \mathbf{v}} + \mathbf{a} \cdot \frac{\partial}{\partial \mathbf{v}} \equiv V_B + V_F. \quad (2.5)$$

To solve (2.3), one takes  $t = n\Delta t$  so that (2.3) can be reduce to  $n$  iterations of the short-time operator  $\exp[\Delta t(T+V_{BF})]$  via Baker-Campbell-Hausdorff type approximations, of which the simplest examples are

$$\begin{aligned} e^{\Delta t(T+V_{BF})} &\approx e^{\Delta t T} e^{\Delta t V_{BF}} \\ &\approx e^{\Delta t T} e^{\Delta t V_B} e^{\Delta t V_F}. \end{aligned} \quad (2.6)$$

The action of each individual operator can easily be computed via series expansion:

$$\begin{aligned} e^{\Delta t T} \begin{pmatrix} \mathbf{r} \\ \mathbf{v} \end{pmatrix} &= \left(1 + \Delta t \mathbf{v} \cdot \frac{\partial}{\partial \mathbf{r}} + \frac{\Delta t^2}{2} (\mathbf{v} \cdot \frac{\partial}{\partial \mathbf{r}})^2 + \dots\right) \begin{pmatrix} \mathbf{r} \\ \mathbf{v} \end{pmatrix} \\ &= \begin{pmatrix} \mathbf{r} + \Delta t \mathbf{v} \\ \mathbf{v} \end{pmatrix} \end{aligned} \quad (2.7)$$

$$\begin{aligned} e^{\Delta t V_F} \begin{pmatrix} \mathbf{r} \\ \mathbf{v} \end{pmatrix} &= \left(1 + \Delta t \mathbf{a} \cdot \frac{\partial}{\partial \mathbf{v}} + \frac{\Delta t^2}{2} (\mathbf{a} \cdot \frac{\partial}{\partial \mathbf{v}})^2 + \dots\right) \begin{pmatrix} \mathbf{r} \\ \mathbf{v} \end{pmatrix} \\ &= \begin{pmatrix} \mathbf{r} \\ \mathbf{v} + \Delta t \mathbf{a} \end{pmatrix}. \end{aligned} \quad (2.8)$$

More generally, the product approximation

$$e^{\Delta t(T+V_F)} = \prod_{i=1}^N e^{a_i \Delta t T} e^{b_i \Delta t V_F} \quad (2.9)$$

with suitable coefficients  $a_i$  and  $b_i$ , then generates sequential updates (2.7) and (2.8), which is a *symplectic integrator*[18–20] of arbitrary order for solving (2.1) without a magnetic field. Since (2.7) and (2.8) are sequential translations, it is obvious that any algorithm of the form (2.9) is phase-volume preserving. Likewise, the approximation

$$e^{\Delta t(T+V_B)} = \prod_{i=1}^N e^{a_i \Delta t T} e^{b_i \Delta t V_B} \quad (2.10)$$

will generate sequential updates which are *exact energy conserving*[15] for solving (2.1) with only a magnetic field. This Lie operator method is powerful in that even without knowing the explicit form of  $\exp(b_i \Delta t V_B)$ , one can prove that (2.10) is exact energy conserving because by (2.7),

$$e^{a_i \Delta t T} \mathbf{v}^2 = \mathbf{v}^2 \quad (2.11)$$

and

$$e^{b_i \Delta t V_B} \mathbf{v}^2 = (1 + b_i \Delta t \omega (\hat{\mathbf{B}} \times \mathbf{v}) \cdot \frac{\partial}{\partial \mathbf{v}} + \dots) \mathbf{v}^2 = \mathbf{v}^2, \quad (2.12)$$

since after differentiating  $\mathbf{v}^2$ , the resulting triple product vanishes. Moreover (2.12) implies that the effect of  $e^{b_i \Delta t V_B}$  on  $\mathbf{v}$  must only be a rotation. Consequently the algorithm (2.10) is a sequence of translations and rotations and therefore again phase-volume preserving. Finally, the approximation

$$e^{\Delta t (T + V_{BF})} = \prod_{i=1}^N e^{a_i \Delta t T} e^{b_i \Delta t V_{BF}} \quad (2.13)$$

will generate sequential updates of a *Poisson integrator*[14, 15] for solving charged particle trajectories in a combined electric and magnetic field to arbitrary precision. Again, even without knowing the explicit form of  $\exp(\Delta t V_{BF}) \mathbf{v}$  it is easy to prove that (2.13) must also be volume preserving. This is because  $\exp(\Delta t V_{BF})$  itself can be approximated to any order of accuracy as

$$e^{\Delta t V_{BF}} = \prod_{i=1}^N e^{a_i \Delta t V_B} e^{b_i \Delta t V_F} \quad (2.14)$$

which is only a sequence of translations and rotations and therefore must be phase-volume preserving.

However, the explicit form of  $\exp(\Delta t V_B) \mathbf{v}$  and  $\exp(\Delta t V_{BF}) \mathbf{v}$  are known from Ref.15,

$$e^{\Delta t V_B} \begin{pmatrix} \mathbf{r} \\ \mathbf{v} \end{pmatrix} = \begin{pmatrix} \mathbf{r} \\ \mathbf{v}_B(\mathbf{r}, \mathbf{v}, \Delta t) \end{pmatrix} \quad (2.15)$$

$$e^{\Delta t V_{BF}} \begin{pmatrix} \mathbf{r} \\ \mathbf{v} \end{pmatrix} = \begin{pmatrix} \mathbf{r} \\ \mathbf{v}_B(\mathbf{r}, \mathbf{v}, \Delta t) + \mathbf{v}_F(\mathbf{r}, \mathbf{v}, \Delta t) \end{pmatrix} \quad (2.16)$$

where

$$\begin{aligned} \mathbf{v}_B(\mathbf{r}, \mathbf{v}, \Delta t) &= \mathbf{v} + \sin \theta (\hat{\mathbf{B}} \times \mathbf{v}) + (1 - \cos \theta) \hat{\mathbf{B}} \times (\hat{\mathbf{B}} \times \mathbf{v}) \\ &= \mathbf{v}_{\parallel} + \cos \theta \mathbf{v}_{\perp} + \sin \theta (\hat{\mathbf{B}} \times \mathbf{v}_{\perp}) \end{aligned} \quad (2.17)$$

$$\mathbf{v}_F(\mathbf{r}, \mathbf{v}, \Delta t) = \Delta t \mathbf{a} + \frac{1}{\omega} (1 - \cos \theta) \hat{\mathbf{B}} \times \mathbf{a} + \Delta t \left(1 - \frac{\sin \theta}{\theta}\right) \hat{\mathbf{B}} \times (\hat{\mathbf{B}} \times \mathbf{a}) \quad (2.18)$$

$$= \Delta t \mathbf{a}_{\parallel} + \frac{1}{\omega} \left[ (1 - \cos \theta) (\hat{\mathbf{B}} \times \mathbf{a}_{\perp}) + \sin \theta \mathbf{a}_{\perp} \right], \quad (2.19)$$

with  $\theta = \omega(\mathbf{r}) \Delta t$  and where  $\mathbf{v}_{\parallel} + \mathbf{v}_{\perp} = \mathbf{v}$ ,  $\mathbf{a}_{\parallel} + \mathbf{a}_{\perp} = \mathbf{a}$  are components parallel and perpendicular to the local magnetic field direction  $\hat{\mathbf{B}}(\mathbf{r})$ . Eq.(2.17) is the effect of  $e^{\Delta t V_B}$  on

$\mathbf{v}$ , which is to rotate only  $\mathbf{v}_\perp$  thereby preserving  $|\mathbf{v}|$  and the kinetic energy. Eq.(2.19) is due to the  $\mathbf{E} \times \mathbf{B}$  drift and will be explained in Sect.V. The program is therefore complete for the generation of arbitrarily accurate magnetic field integrators (2.10) or (2.13) in the limit of small  $\Delta t$ . The goal of this work, however is to show how Boris solvers can also be derived from this powerful machinery and to seek accurate integrators for solving magnetic field trajectories in the regime of *large*  $\Delta t$ .

### III. FIRST-ORDER MAGNETIC FIELD INTEGRATORS

Boris[2] originally derived his solver by modifying the implicit midpoint method. Here, we will show how Boris solvers can be derived from last Section's Lie operator method independent of finite-difference schemes. For clarity we will begin with magnetic field only integrators of the form (2.10). The two basic first-order approximations are

$$\mathcal{T}_{1A} = e^{\Delta t V_B} e^{\Delta t T} \quad \text{and} \quad \mathcal{T}_{1B} = e^{\Delta t T} e^{\Delta t V_B} \quad (3.1)$$

producing the following two sequential *magnetic* field integrators M1A,

$$\begin{aligned} \mathbf{v}_1 &= \mathbf{v}_B(\mathbf{r}_0, \mathbf{v}_0, \Delta t) \\ \mathbf{r}_1 &= \mathbf{r}_0 + \Delta t \mathbf{v}_1 \end{aligned} \quad (3.2)$$

and M1B,

$$\begin{aligned} \mathbf{r}_1 &= \mathbf{r}_0 + \Delta t \mathbf{v}_0 \\ \mathbf{v}_1 &= \mathbf{v}_B(\mathbf{r}_1, \mathbf{v}_0, \Delta t). \end{aligned} \quad (3.3)$$

(Note that the operators act from right to left, resulting in variables being updated as if according to operators from left to right.) Eq.(2.17) shows that the local magnetic field simply rotates the perpendicular velocity component by  $\theta = \omega(\mathbf{r})\Delta t$ , leaving its parallel component and magnitude unchanged. M1A first rotates  $\mathbf{v}_0$  by  $\theta$  then moves to the new position along the rotated velocity. M1B first moves to the new position using the present velocity, then rotates it after arrival. In our naming scheme, the suffix A or B denotes the algorithm whose first step is updating the velocity or the position, respectively.

The working of these two algorithms is extremely easy to analyze for a negatively charged particle in a constant magnetic field in the  $\hat{\mathbf{z}}$  direction, as shown in Fig.1. When the particle

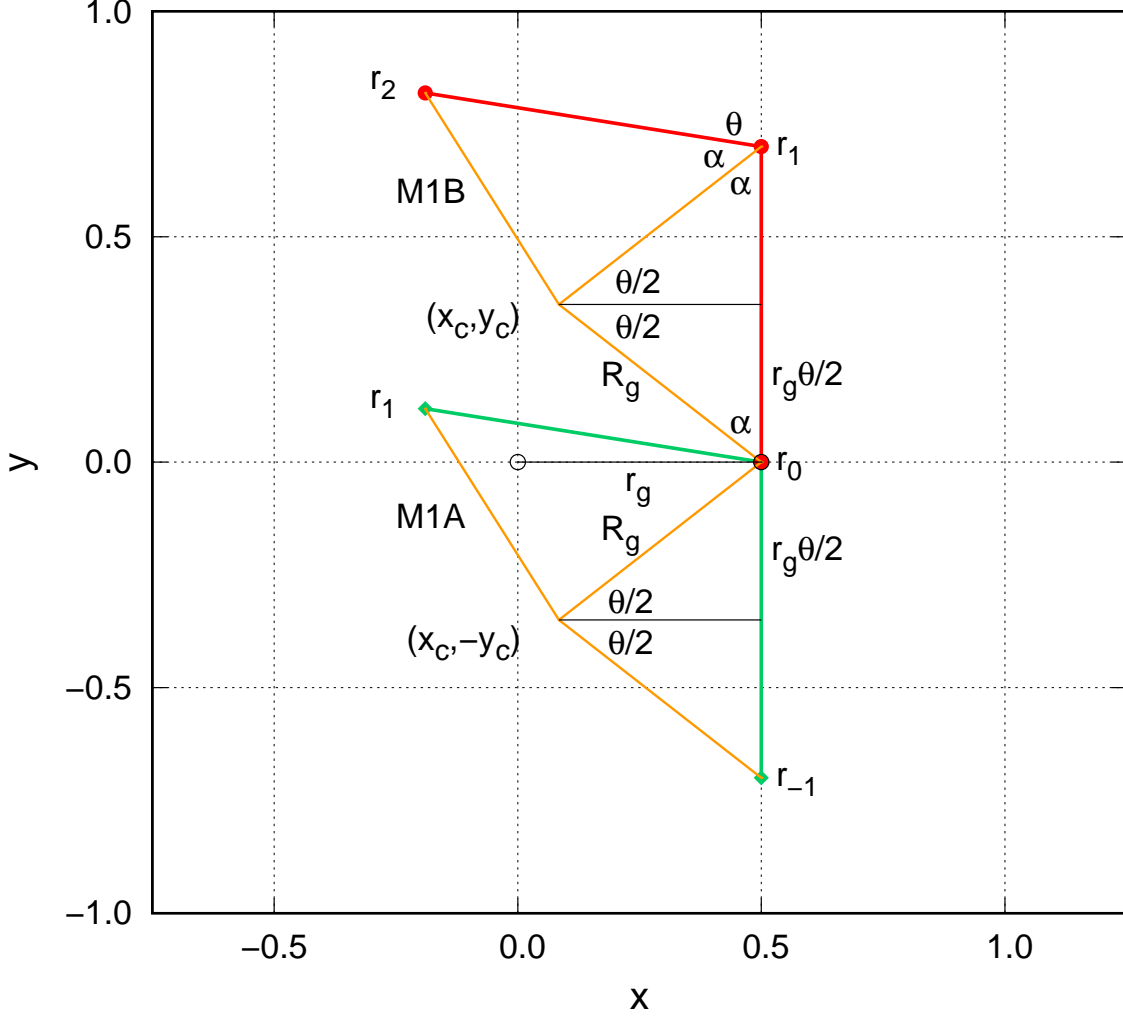


FIG. 1. (color online) The anatomy of first-order Poisson solvers M1A and M1B.

is at  $\mathbf{r}_0$ , moving with tangential velocity  $\mathbf{v}_0$  on the gyro-circle with radius  $r_g = v_0/\omega$ , M1B would move it in time  $\Delta t$ , a distance  $v_0\Delta t = r_g\theta$  to  $\mathbf{r}_1$ . At  $\mathbf{r}_1$ , it would rotate the velocity from the vertical by  $\theta$  and move it to  $\mathbf{r}_2$ . Since both  $\mathbf{r}_0$  and  $\mathbf{r}_1$  must be on the algorithm's gyro-circle of radius  $R_g$  centered at  $(x_c, y_c)$ , both must be equidistant from  $(x_c, y_c)$ . This means that  $(x_c, y_c)$  must lie on the perpendicular bisector of  $\mathbf{r}_1 - \mathbf{r}_0$ , and therefore

$$y_c = r_g\theta/2. \quad (3.4)$$

At  $\mathbf{r}_1$ ,  $\theta$  is the rotation angle from the vertical and the supplementary angle to it is  $2\alpha$ . Since  $\theta + 2\alpha = \pi \rightarrow \theta/2 + \alpha = \pi/2$ , the bisector's angle with either  $R_g$  on its sides is  $\theta/2$

and therefore  $R_g \sin(\theta/2) = r_g \theta/2$ , or

$$R_g = r_g \frac{\theta/2}{\sin(\theta/2)} = r_g \left(1 + \frac{\theta^2}{24} + \dots\right). \quad (3.5)$$

This also means that the length of the bisector is  $R_g \cos(\theta/2)$  and hence

$$\begin{aligned} x_c &= r_g - R_g \cos(\theta/2) \\ &= r_g \left(1 - \frac{\theta/2}{\tan(\theta/2)}\right) = r_g \left(\frac{\theta^2}{12} + \dots\right). \end{aligned} \quad (3.6)$$

Note that since  $\theta/2 + \alpha = \pi/2$ , if one were to rotate  $\mathbf{r}_1 - \mathbf{r}_0$  by  $\theta/2$ , then  $y_c = 0$ . Also, if one shifts  $y \rightarrow y - r_g \theta/2$  by starting out at the midpoint of  $\mathbf{r}_1 - \mathbf{r}_0$ , then also  $y_c = 0$ . These cases are discussed in the next Section.

Similarly, for M1A, in order for the velocity to be rotated at  $\mathbf{r}_0$ , its previous position must be at  $\mathbf{r}_{-1}$ . It therefore follows that the y-coordinate of its gyro-center must be

$$y_c = -r_g \theta/2 \quad (3.7)$$

but with the same  $R_g$  and  $x_c$  as given by (3.5) and (3.6). Eq.(3.4)-(3.7) are the defining properties of these two fundamental algorithms. These are all errors, since for the exact trajectory, one must have  $x_c = y_c = 0$  and  $R_g = r_g$ . As expected, the first-order (in  $\Delta t$ ) errors  $y_c = \pm r_g \theta/2$  are odd and opposite in sign, while those of second-order,  $x_c$  and  $R_g$ , are the same and even in  $\Delta t$ .

Normally, one would need higher-order methods to eliminate these  $\Delta t$ -dependent errors. However, trajectories in a constant magnetic field have two distinct motions: translation by  $v_0 \Delta t = r_g \theta$  and rotation by angle  $\theta = \omega \Delta t$ . It is only because  $v_0$  remains unchanged in a constant magnetic field that both motions are proportional to the same  $\theta$ . In principle, and in conventional dynamics, there is no such coupling between the two motions that would force the same  $\theta$  on both. One therefore has this residual freedom of decoupling both motion to reduce these errors. *This is the foundational insight by which this work explains the existence of Boris solvers*, which is distinct from conventional derivations based on *ad hoc* modifications of finite-difference schemes.

First, one can decouple the rotation angle in trigonometric functions from  $\theta$  to an effective angle  $\theta_B(\theta)$ . From (3.6), the choice of

$$\tan(\theta_B/2) = \theta/2 \quad (3.8)$$



would force  $x_c = 0$ . If  $x_c = 0$ , then from Fig.1,  $R_g$  is the hypotenuse of a right triangle with base  $r_g$  and height  $r_g\theta/2$ :

$$R_g = r_g \sqrt{1 + \frac{\theta^2}{4}}. \quad (3.9)$$

This choice (3.8) means that for (3.2) and (3.3), the rotation angle  $\theta$  in (2.17) is to be replaced by the Boris angle  $\theta_B$ , yielding

$$\mathbf{v}_B(\mathbf{r}, \mathbf{v}, \Delta t) = \mathbf{v}_{\parallel} + \cos \theta_B \mathbf{v}_{\perp} + \sin \theta_B (\hat{\mathbf{B}} \times \mathbf{v}_{\perp}) \quad (3.10)$$

with

$$\sin \theta_B = \frac{2 \tan(\theta_B/2)}{1 + \tan^2(\theta_B/2)} = \frac{\theta}{1 + \theta^2/4} \quad (3.11)$$

$$\cos \theta_B = \frac{1 - \tan^2(\theta_B/2)}{1 + \tan^2(\theta_B/2)} = \frac{1 - \theta^2/4}{1 + \theta^2/4}. \quad (3.12)$$

This rotation angle replacement  $\theta \rightarrow \theta_B$  in M1A and M1B then produces leap-frog Boris solvers B1A and B1B.

Second, from (3.5) one can force  $R_g = r_g$  by defining a new angle  $\theta_C$ , such that

$$\sin(\theta_C/2) = \theta/2, \quad \cos(\theta_C/2) = \sqrt{1 - \theta^2/4}, \quad (3.13)$$

and consequently,

$$\sin \theta_C = \theta \sqrt{1 - \theta^2/4}, \quad \cos \theta_C = (1 - \theta^2/2). \quad (3.14)$$

In this case,

$$x_c = r_g(1 - \cos(\theta/2)) = r_g(1 - \sqrt{1 - (\theta/2)^2}), \quad (3.15)$$

which limits the algorithm to  $|\theta| \leq 2$ . The resulting algorithms (3.2) and (3.3) with rotation angle  $\theta_C$  are previously unknown Boris solvers and will be referred to as C1A and C1B.

To see the working of these algorithms, consider the case of an electron in a constant magnetic field with  $\omega = 2$ ,  $\hat{\mathbf{B}} = \hat{\mathbf{z}}$ ,  $\mathbf{r} = (x, y)$ ,  $\mathbf{v} = \mathbf{v}_{\perp} = (v_x, v_y)$ , with initial velocity  $\mathbf{v}_0 = (0, v_0)$ ,  $\mathbf{r}_0 = (r_g, 0)$ , where  $v_0 = 1$  and where  $r_g = v_0/\omega = 1/2$  is the gyro-radius. Take a large  $\Delta t = \pi/4$ ,  $\theta = \omega\Delta t = \pi/2$  so that the trajectory of both M algorithms would rotate through  $90^\circ$  4 times to complete one orbit. These are the two (red) square orbits shown in Fig.2. The two blue and green orbits are those of B and C solvers. Their orbits are tilted backward and forward as compare to the M algorithms because their decoupling angle

$$\begin{aligned} \theta_B &= 2 \tan^{-1}(\theta/2) = \theta - \frac{\theta^3}{12} + \dots \\ \theta_C &= 2 \sin^{-1}(\theta/2) = \theta + \frac{\theta^3}{24} + \dots \end{aligned} \quad (3.16)$$

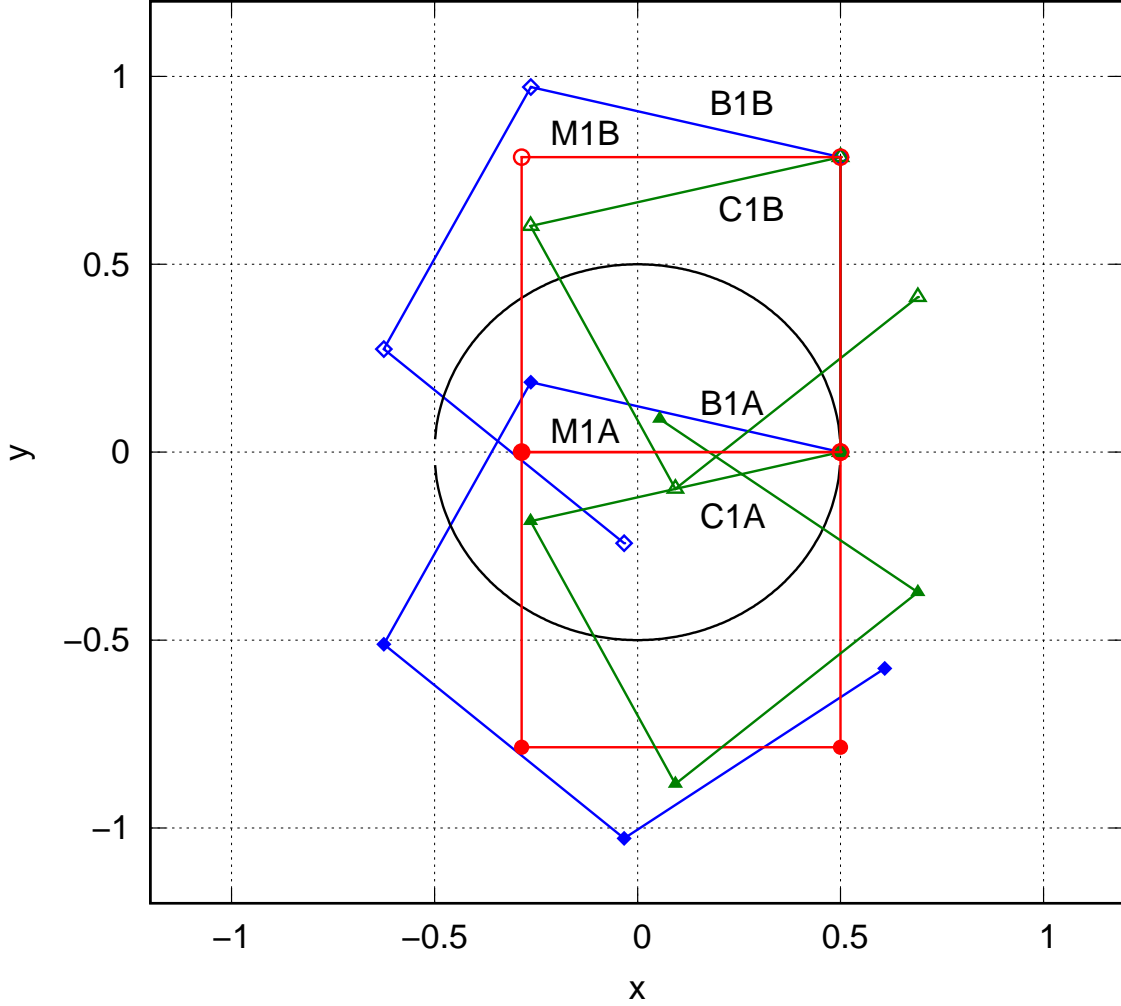


FIG. 2. (color online) The orbits of six first-order magnetic field algorithms at a large  $\Delta t = \pi/4$ .

lags or leads the correct angle.

Since these six integrators only rotate the velocity vector, all are exact energy conserving for a general magnetic field. Since they are sequential, they are structurally identical to leap-frog algorithms. In the limit of  $\Delta t \rightarrow 0$ , all six algorithms will converge onto the exact gyro-orbit. All are only first-order because the convergence of the gyro-center coordinate  $y_c = \pm r_g \theta / 2$  is linear in  $\Delta t$ .

In the limit of large  $\Delta t$ , the C algorithms are limited to  $\Delta t \leq 2/\omega$ , otherwise,  $\theta_C$  cannot be defined by (3.13). For the M algorithms, their gyro-radius (3.5) can be arbitrarily large near  $\theta = n2\pi$  and is always  $\geq r_g \theta / 2$ . For the B algorithms, their gyro-radii given by (3.9) grow linearly as  $r_g \theta / 2$  at large  $\Delta t$ .

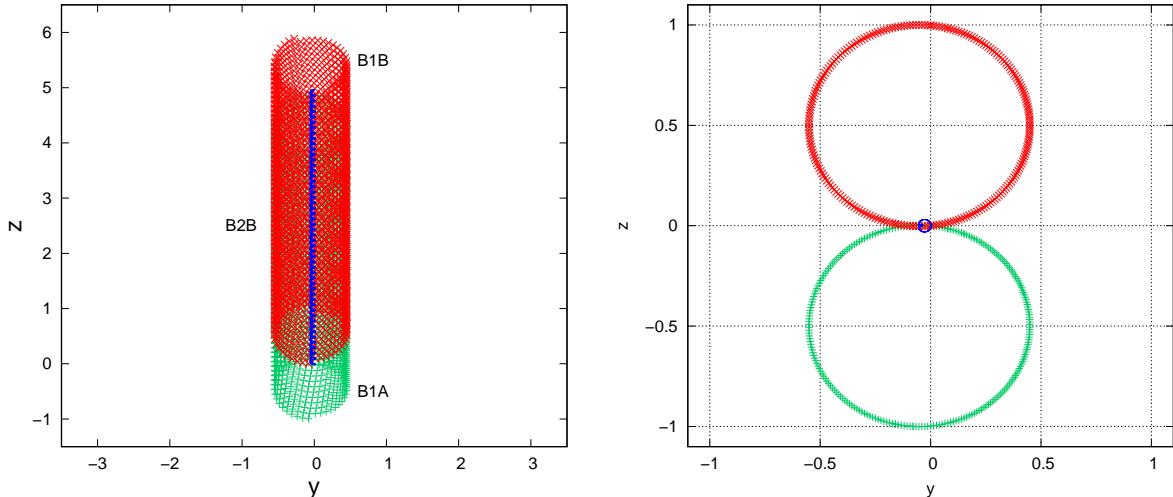


FIG. 3. (color online) **Left** (a): Trajectories of solvers B1A, B1B, and B2B at  $\Delta t = 0.5$ , reproducing Parker and Birdsall's [4] gradient B drift calculation Fig.3. **Right** (b): Collapsing the trajectories by removing the vertical drift in  $z(t)$ . See text for details.

To see which of the B algorithm has been historically regarded as “the Boris solver”, we apply B1A and B1B to the case of a non-uniform magnetic field  $\mathbf{B} = (100 - 25y)\hat{\mathbf{x}}$ , taken from Parker and Birdsall's [4] Fig.3, with  $\mathbf{r}_0 = (0, 0, 0)$  and  $\mathbf{v}_0 = (0, 0, 2)$ . For this case, near  $y = 0$ ,  $\omega = 100$ ,  $\Delta t = 0.5$ ,  $\theta = 50$ ,  $2r_g = 4/100 = 0.04$ ,  $2R_g = 1.0008$  and  $y_c = \pm r_g \theta / 2 = \pm 0.5$ . The resulting trajectories are as shown in Fig.3(a). By comparing Fig.3(a) to Parker and Birdsall's [4] Fig.3, one can readily see that Parker and Birdsall's Boris solver is B1B, since its gyro-center is 0.5 above the nearly exact trajectory of B2B. By removing the vertical drift of  $0.004941t$  (rather than  $0.005t$ ), the trajectories collapse back onto themselves as shown in Fig.3(b). Both the  $y_c$  off-set and the gyro-radius for B1A and B1B are as predicted. There is also a slight horizontal off-set of  $\approx -0.05$  due to higher order effects of the nonuniform magnetic field.

The solver B2B will be derived and further discussed in the next section. Its collapsed trajectory is truly a cycloid, with a maximum horizontal separation of exactly  $2r_g = 0.04$ , but a vertical diameter of  $\approx 0.06$ . Its gyro-radius is therefore much closer to the exact and  $\approx 20$  times smaller than those of B1A and B1B in Fig.3(b). (It may not be visible unless the figure is greatly magnified.)

Next, we check all three solvers against Parker and Birdsall's [4] curvature drift calculation due to a magnetic field  $\mathbf{B}(\mathbf{r}) = (800/r)\hat{\boldsymbol{\theta}}$  from a line current flowing along  $\hat{\mathbf{z}}$  at  $\mathbf{r} = (10, 10, 0)$

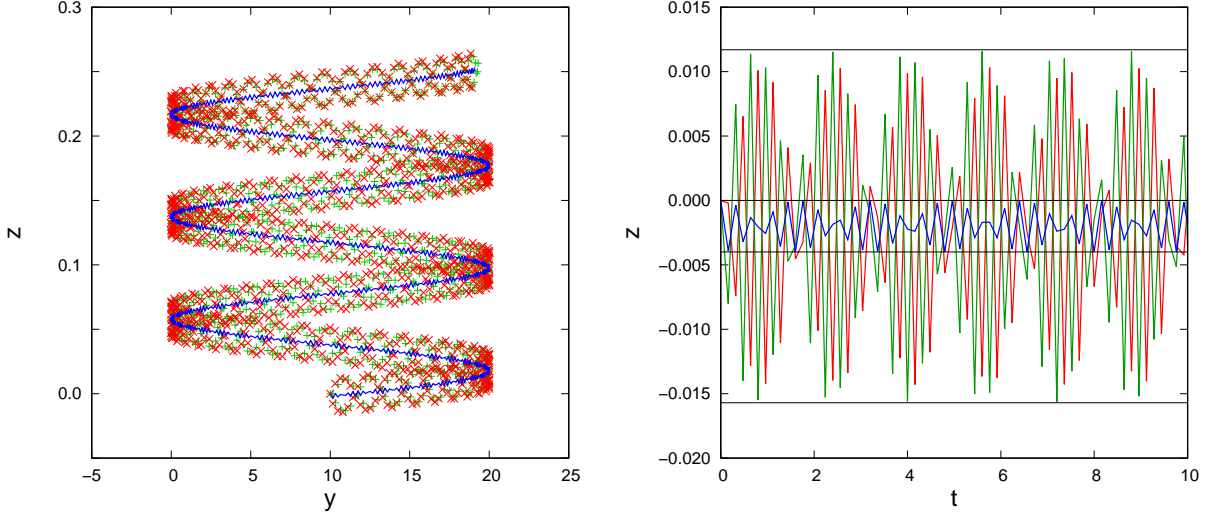


FIG. 4. (color online) **Left** (a): Trajectories from B1A (green), B1B (red) and B2B (blue) at  $\Delta t = 0.16$ , reproducing Parker and Birdsall's[4] Fig.2. **Right** (b): Oscillations of  $z(t)$  after removing the vertical drift.

with  $\mathbf{r}_0 = (0, 10, 0)$  and  $\mathbf{v}_0 = (0.16, 1, 0)$ . The time step is nearly twice the gyro-period at the starting position. B1A's and B1B's oscillating trajectories basically intertwine, with no discernible off-sets. B2B's oscillations are much smaller. The oscillation sizes can again be determined by removing the vertical drift ( $0.0012648t$ ) in Fig.4(b). For  $z$  along  $\mathbf{r} = (10, 10, z)$ ,  $\omega = 80$ ,  $v_{\perp} = 0.16$ , the gyro-radius is  $0.16/80 = 0.002$ . As shown in Fig.4(b), B2B's oscillation is precisely within the gyro-diameter of  $0.004$ . At  $\Delta t = 0.16$ ,  $\theta = \omega\Delta t = 12.8$ , the first-order gyro-diameter is  $2R_g = 0.0259$ . The top and bottom lines in Fig.4(b) are at  $z = 0.0116$  and  $z = -0.0156$  respectively, giving a diameter of  $0.0272$  for B1A. Similarly, the oscillating width of B1B can be determined to be  $0.0247$ . Surprisingly, their average is  $\approx 0.0259$ , in excellent agreement with  $2R_g$ . (This is similar to the case of the polarization drift in Sect.V.) Again, B2B tracks the correct local gyro-circle at large values of  $\Delta t$  an order of magnitude better than B1A or B1B.

Any work which cites (3.9) as the solver's gyro-radius must have only understood the Boris solver as either B1A or B1B, as in Refs.3-7, 10, and 12. There is no such  $\Delta t$ -dependent gyro-radius error in B2B.

#### IV. SECOND-ORDER MAGNETIC FIELD INTEGRATORS

Except for the faster evaluations of rotations via (3.11), (3.12) or (3.14), there does not appear to be any qualitative advantage of using the B or C algorithms over M1A or M1B. Moreover, as shown in Fig.3, at large  $\Delta t$ , B1A and B1B have huge first-order off-set error  $y_c = \pm r_g \theta/2$ . However, it is well known in sequential integrators[18, 20] that first-order errors are eliminated by a time-symmetric concatenation of the two first-order methods,

$$\mathcal{T}_{2A} = e^{(\Delta t/2)V_B} e^{\Delta t T} e^{(\Delta t/2)V_B} \quad \text{and} \quad \mathcal{T}_{2B} = e^{(\Delta t/2)T} e^{\Delta t V_B} e^{(\Delta t/2)T} \quad (4.1)$$

yielding the following second-order integrators M2A,

$$\begin{aligned} \mathbf{v}_1 &= \mathbf{v}_B(\mathbf{r}_0, \mathbf{v}_0, \Delta t/2) \\ \mathbf{r}_1 &= \mathbf{r}_0 + \Delta t \mathbf{v}_1 \\ \mathbf{v}_2 &= \mathbf{v}_B(\mathbf{r}_1, \mathbf{v}_1, \Delta t/2) \end{aligned} \quad (4.2)$$

and M2B,

$$\begin{aligned} \mathbf{r}_1 &= \mathbf{r}_0 + \frac{1}{2} \Delta t \mathbf{v}_0 \\ \mathbf{v}_1 &= \mathbf{v}_B(\mathbf{r}_1, \mathbf{v}_0, \Delta t) \\ \mathbf{r}_2 &= \mathbf{r}_1 + \frac{1}{2} \Delta t \mathbf{v}_1. \end{aligned} \quad (4.3)$$

For the same test problem as in Fig.2, they now produce the two upright square orbits as labeled in Fig.5. The off-set errors  $y_c = \pm r_g \theta/2$ , so glaring in Fig.3(b), are now gone.

The anatomy of these two algorithms are shown in Fig.6. For M2A, the particle starts at  $\mathbf{r}_0$ , rotates by  $\theta/2$ , then travels the full distance  $r_g \theta$  to  $\mathbf{r}_1$ . This is just  $\mathbf{r}_1 - \mathbf{r}_0$  of M1B rotated by  $\theta/2$  and therefore  $y_c = 0$ . One then has the bottom right triangle with

$$\sin(\theta/2) = \frac{r_g(\theta/2)}{R_g} \quad \rightarrow \quad R_g = r_g \frac{\theta/2}{\sin(\theta/2)} \quad (4.4)$$

and again

$$x_c = r_g - R_g = r_g \left(1 - \frac{\theta/2}{\sin(\theta/2)}\right). \quad (4.5)$$

For the case in Fig.5,  $x_c = (1 - \pi\sqrt{2}/4)/2 \approx -0.05536$ , which is correct.

In contrast to the first order case, the alternative Boris angle  $\sin(\theta_C/2) = \theta/2$  now forces *both*  $R_g = r_g$  and  $x_c = 0$ . This means that if  $\mathbf{r}_0$  is initially at the gyro-circle, then  $\mathbf{r}_1$ , and all subsequent positions must also be on the gyro-circle, as long as  $|\theta/2| \leq 1$ . We will refer to

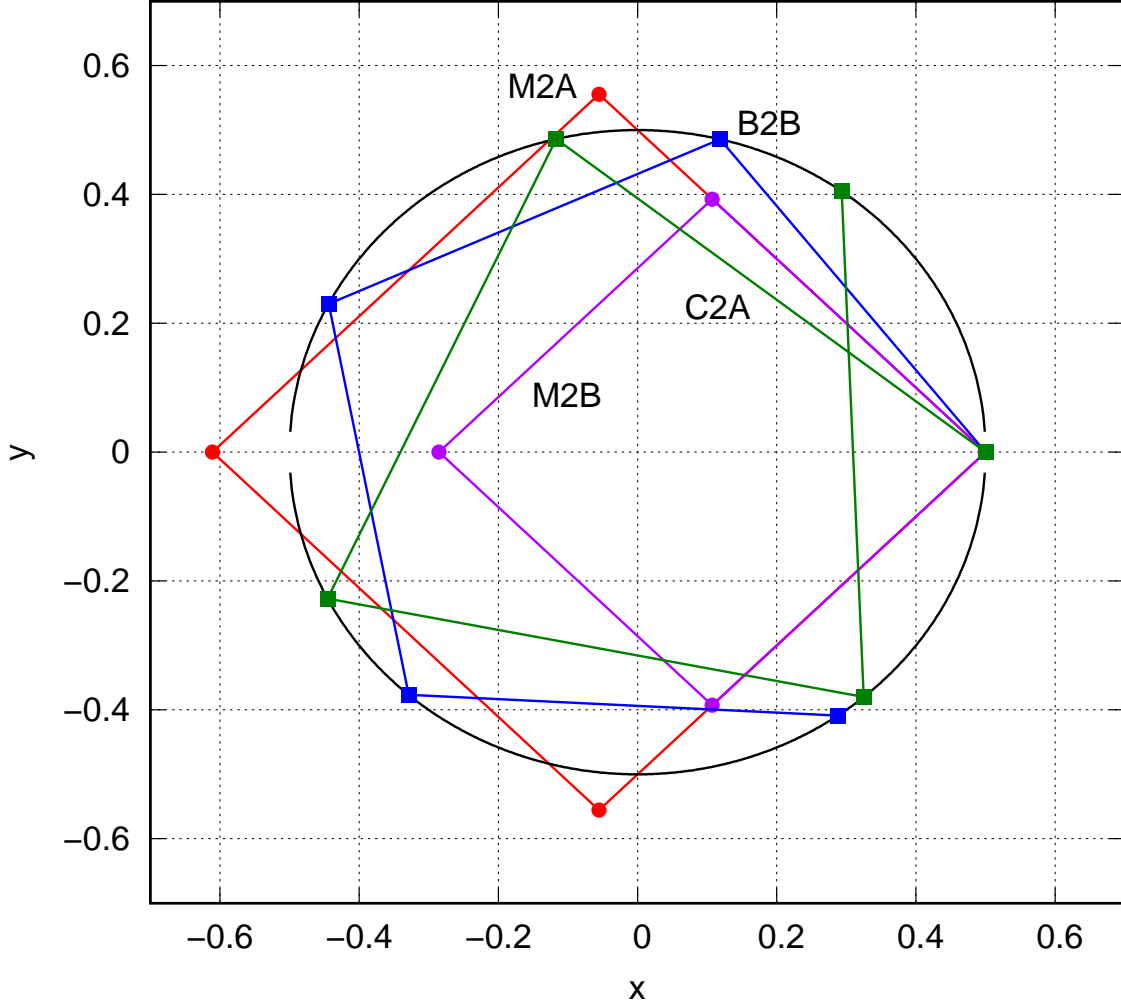


FIG. 5. (color online) For the same configuration as Fig.2, the two second-order algorithms M2A and M2B produce two square orbits having the correct rotation angles. C2A and B2B are the two second-order Boris solvers with trajectories exactly on the gyro-circle but with out-of-phase rotation angles.

this algorithm as C2A. Note that for C2A, only its defining angle (3.13) is needed in (4.2), not its double angle (3.14).

Similarly, for M2B, the particle starts at  $\mathbf{r}_0$ , moves along  $\mathbf{v}_0$  a distance  $r_g\theta/2$  to  $\mathbf{r}_1$ , rotates  $\mathbf{v}_0$  by  $\theta$ , then travels  $r_g\theta/2$  again to  $\mathbf{r}_2$ . The points  $\mathbf{r}_0$  and  $\mathbf{r}_2$  here are just midpoints of M1B with shifted  $y \rightarrow y - r_g\theta/2$ , therefore automatically giving  $y_c = 0$ . From the base triangle, one now has

$$\tan(\theta/2) = r_g(\theta/2)/R_g \quad \rightarrow \quad R_g = r_g \frac{\theta/2}{\tan(\theta/2)} \quad (4.6)$$

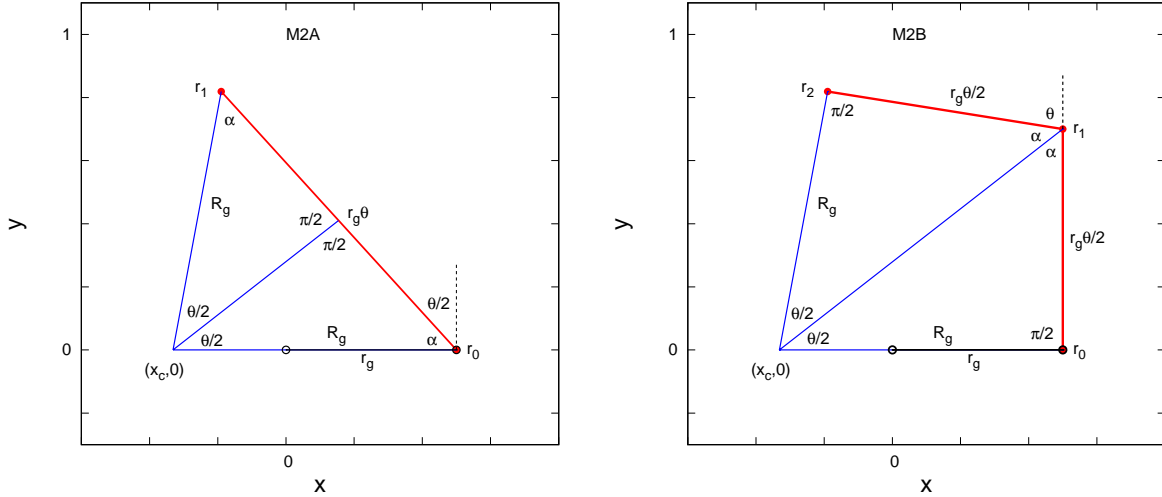


FIG. 6. (color online) The anatomy of second-order Poisson solvers M2A and M2B.

and

$$x_c = r_g - R_g = r_g \left(1 - \frac{\theta/2}{\tan(\theta/2)}\right). \quad (4.7)$$

For M2B in Fig.5,  $x_c = (1 - \pi/4)/2 \approx 0.10730$ , which is also correct. The choice of the original Boris angle  $\tan(\theta_B/2) = \theta/2$  then also forces both  $R_g = r_g$  and  $x_c = 0$ , yielding trajectories that are exactly on the gyro-circle for *all*  $\Delta t$ . We will refer to this algorithm as B2B. The trajectories of C2A and B2B are as shown in Fig.5. The rotation angles of M2A and M2B are again exactly correct, while those of C2A and B2B are ahead and behind by approximately the same amount.

Algorithms B2A and C2B, corresponding to choosing the wrong Boris angle for M2A and M2B will not yield trajectories on the gyro-circle. They are just phase-shifted versions of M2A and M2B and therefore not shown in Fig.5. All six algorithms will converge as second-order integrators at small  $\Delta t$ . However, one perennial problem of plasma physics simulations is that one would like to use time steps not limited by the rapid local cyclotron motion and short gyro-period. The Boris solver B2B is unique in that in the limit of  $\theta \rightarrow \infty$ ,  $\theta_B \rightarrow \pi$ , B2B's trajectory will just bounce back and forth nearly as straight lines across the diameter of the gyro-circle. Thus in contrast to all other algorithms, only B2B's trajectory remains bounded to the exact orbit even as  $\Delta t \rightarrow \infty$ . As shown in Figs.3 and 4, its gyro-radius remains nearly identical to the exact result even for a non-uniform magnetic field and is orders of magnitude smaller than those of B1A and B1B.

In a recent work, one of us has given an alternative derivation[13] of C2A and B2B

by requiring M2A's and M2B's trajectory to be exactly on the gyro-circle. That then automatically forces the gyro-center to the origin and  $R_g = r_g$ . That derivation did not explain why one has to start with M2A and M2B. The present derivation shows that the gyro-centers of first-order algorithms M1A and M1B are off set at  $(x_c, y_c)$ . The first-order error  $y_c$  must first be eliminate by symmetrizing the algorithms into second-order solvers M2A and M2B. Second-order errors in  $x_c$  and  $R_g$  can then be eliminated simultaneously by a suitable choice of the Boris angle, resulting in on-orbit trajectories. The two derivations are therefore complementary. A third derivation of C2A and B2B has been implicitly given in Ref.15 sometime ago. For completeness, that derivation will now be summarized in Appendix A.

Algorithm B2B is cited as the Boris solver in Refs.8, 9, 11, and 14. The fact that its trajectory in a constant magnetic field is exactly on the gyro-circle seemed not to be widely known after Boris superseded Buneman's derivation[3], otherwise, it would not have been necessary for Stoltz, Cary, Penn and Wurtele[8] to explicitly verify that again in 2002. This on-orbit property is also not noted in some recent publications[10–12].

## V. SECOND-ORDER ELECTRIC AND MAGNETIC FIELD INTEGRATORS

For a general electric and magnetic field, second order algorithms given by (2.13) are

$$\mathcal{T}_{2A} = e^{(\Delta t/2)V_{BF}} e^{\Delta t T} e^{(\Delta t/2)V_{BF}} \quad \text{and} \quad \mathcal{T}_{2B} = e^{(\Delta t/2)T} e^{\Delta t V_{BF}} e^{(\Delta t/2)T} \quad (5.1)$$

which will be named as EM2A and EM2B. Since the action of  $e^{\Delta t V_{BF}}$  on  $\mathbf{r}$  and  $\mathbf{v}$  are known via (2.16), the algorithms are straightforwardly defined. However, we will give here a more intuitive treatment, in order to explain the meaning of (2.19).

Since motions parallel to the magnetic field are trivial, without loss of generality, one can assume that both  $\mathbf{v}$  and  $\mathbf{a}$  are perpendicular to  $\mathbf{B}$ . To solve (2.1), one can set

$$\mathbf{v} = \tilde{\mathbf{v}} + \mathbf{u} \quad \text{with} \quad \mathbf{u} = \frac{1}{\omega} \hat{\mathbf{B}} \times \mathbf{a} \quad (5.2)$$

where  $\mathbf{u}$  is the constant  $\mathbf{E} \times \mathbf{B}$  drift during the integration of (2.1) so that

$$\frac{d\tilde{\mathbf{v}}}{dt} = \omega \hat{\mathbf{B}} \times \tilde{\mathbf{v}} \quad (5.3)$$

with solution

$$\tilde{\mathbf{v}}(\Delta t) = \cos \theta \tilde{\mathbf{v}} + \sin \theta (\hat{\mathbf{B}} \times \tilde{\mathbf{v}}) \equiv R(\mathbf{r}, \Delta t) \tilde{\mathbf{v}} \quad (5.4)$$



which is a pure rotation as indicated. Algorithm EM2B is then

$$\mathbf{r}_1 = \mathbf{r}_0 + \frac{1}{2}\Delta t(\tilde{\mathbf{v}}_0 + \mathbf{u}) \quad (5.5)$$

$$\mathbf{v}_1 = R(\mathbf{r}_1, \Delta t)\tilde{\mathbf{v}}_0 + \mathbf{u} \quad (5.6)$$

$$\mathbf{r}_2 = \mathbf{r}_1 + \frac{1}{2}\Delta t\mathbf{v}_1. \quad (5.7)$$

The final position is therefore

$$\mathbf{r}_2 = \mathbf{r}_0 + \Delta t\mathbf{u} + \frac{1}{2}\Delta t(\tilde{\mathbf{v}}_0 + R_1\tilde{\mathbf{v}}_0), \quad (5.8)$$

which is a cycloid moving with constant drift velocity  $\mathbf{u}$ . Without the drift, (5.8) is just M2B (4.3). If  $\theta \rightarrow \theta_B$  in  $R(\mathbf{r}, \Delta t)$ , then one has B2B. With the drift, (5.5)-(5.7) can be further simplified. The first step (5.5) can be restored to  $\mathbf{r}_1 = \mathbf{r}_0 + \frac{1}{2}\Delta t\mathbf{v}_0$ . The middle step is

$$\mathbf{v}_1 = R(\mathbf{r}_1, \Delta t)(\mathbf{v}_0 - \mathbf{u}) + \mathbf{u} \quad (5.9)$$

$$\begin{aligned} &= R(\mathbf{r}_1, \Delta t)\mathbf{v}_0 + \mathbf{u} - \cos\theta\mathbf{u} - \sin\theta(\hat{\mathbf{B}} \times \mathbf{u}) \\ &= R(\mathbf{r}_1, \Delta t)\mathbf{v}_0 + \frac{1}{\omega}[(1 - \cos\theta)\hat{\mathbf{B}} \times \mathbf{a} + \sin\theta\mathbf{a}]. \end{aligned} \quad (5.10)$$

Eq.(5.9) is the cycloid fitting step of Buneman[1], where he stopped. Here, we go beyond Buneman to (5.10) by taking advantage of the fact that rotation is linear in the velocity. Eq.(5.10) is precisely (2.17) and (2.19) without the parallel motion. Crucially, we now show that (5.10) is identical to Boris'  $\mathbf{E}$  and  $\mathbf{B}$  splitting  $\mathbf{v}_3$  below

$$\begin{aligned} \mathbf{v}_1 &= \mathbf{v}_0 + \frac{1}{2}\Delta t\mathbf{a} \\ \mathbf{v}_2 &= R(\mathbf{r}_1, \Delta t)\mathbf{v}_1 \end{aligned} \quad (5.11)$$

$$\mathbf{v}_3 = \mathbf{v}_2 + \frac{1}{2}\Delta t\mathbf{a} \quad (5.12)$$

if the rotation angle in (5.11) is  $\theta_B$ ! The final velocity (5.12) is

$$\begin{aligned} \mathbf{v}_3 &= R(\mathbf{r}_1, \Delta t)(\mathbf{v}_0 + \frac{1}{2}\Delta t\mathbf{a}) + \frac{1}{2}\Delta t\mathbf{a} \\ &= R(\mathbf{r}_1, \Delta t)\mathbf{v}_0 + \frac{1}{2}\Delta t(\cos\theta_B\mathbf{a} + \sin\theta_B\hat{\mathbf{B}} \times \mathbf{a}) + \frac{1}{2}\Delta t\mathbf{a} \\ &= R(\mathbf{r}_1, \Delta t)\mathbf{v}_0 + \frac{1}{\omega}\left(\frac{1}{2}\theta(1 + \cos\theta_B)\mathbf{a} + \frac{1}{2}\theta\sin\theta_B\hat{\mathbf{B}} \times \mathbf{a}\right). \end{aligned} \quad (5.13)$$

From (3.11) and (3.12), one finds

$$\frac{1}{2}\theta(1 + \cos\theta_B) = \sin\theta_B \quad \text{and} \quad \frac{1}{2}\theta\sin\theta_B = 1 - \cos\theta_B, \quad (5.14)$$

and therefore (5.13) exactly matches (5.10). Replace (5.10) by this splitting then yields the second order Boris solver EB2B for a general  $\mathbf{E}$  and  $\mathbf{B}$  (including parallel motions)

$$\begin{aligned}
\mathbf{r}_1 &= \mathbf{r}_0 + \frac{1}{2}\Delta t\mathbf{v}_0 \\
\mathbf{v}_1 &= \mathbf{v}_0 + \frac{1}{2}\Delta t\mathbf{a}(\mathbf{r}_1) \\
\mathbf{v}_2 &= \mathbf{v}_B(\mathbf{r}_1, \mathbf{v}_1, \Delta t) \\
\mathbf{v}_3 &= \mathbf{v}_2 + \frac{1}{2}\Delta t\mathbf{a}(\mathbf{r}_1) \\
\mathbf{r}_2 &= \mathbf{r}_1 + \frac{1}{2}\Delta t\mathbf{v}_3.
\end{aligned} \tag{5.15}$$

Removing the first position update and combined it with the last will be designated as EB1A. Removing the last position update and combined it with the first will be designated as EB1B. The fact that the splitting of the electric force from the magnetic is exact for the Boris solver B2B has also been proved by Knapp, Kendl, Koskela and Ostermann[14], using the Cayley form of the Boris rotation. This makes the original Boris solver B2B unique, because this splitting is not true for C2A, *i.e.*, (5.14) is not true for  $\theta_C$ .

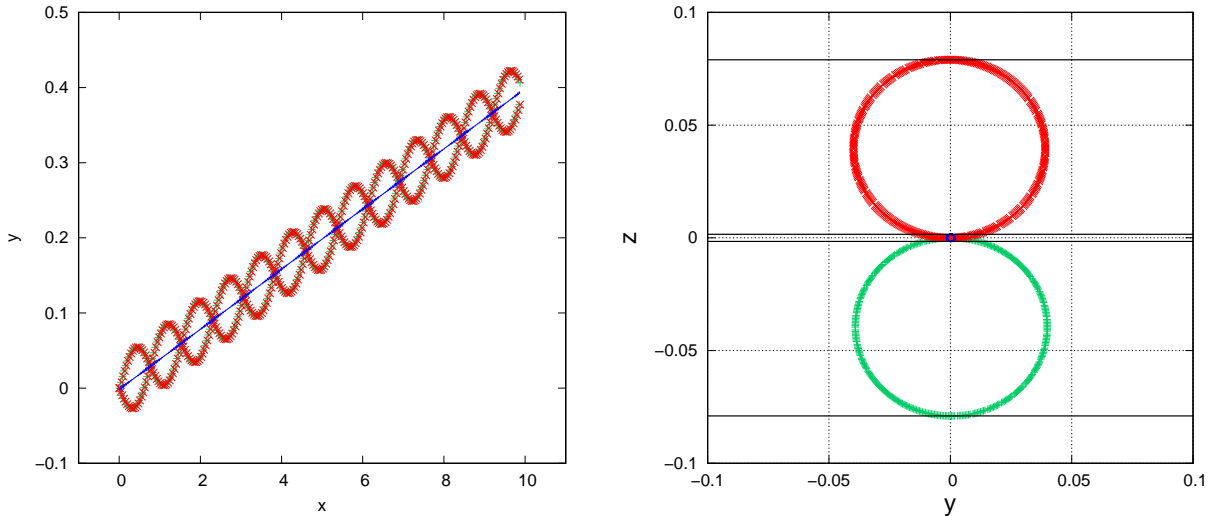


FIG. 7. (color online) **Left** (a):  $\mathbf{E} \times \mathbf{B}$  drift calculation using EB1A (green), EB1B (red) and EB2B (blue) at  $\Delta t = 0.1975$ . **Right** (b): After removing the  $\mathbf{E} \times \mathbf{B}$  drift in the y-direction, the oscillation in the z coordinate reveals the gyro-center location and gyro-radius of all three solvers. See text for details.

In Fig.7(a), we use EB1A, EB1B and EB2B to compute an electron's trajectory in a combined  $\mathbf{E} = \hat{z}$  and  $\mathbf{B} = 250\hat{x}$  field with  $\omega = B = 250$ ,  $\mathbf{a} = -\hat{z}$ ,  $\mathbf{r}_0 = \mathbf{0}$  and  $\mathbf{v}_0 =$

$0.1\hat{\mathbf{x}} + 0.4\hat{\mathbf{z}}$ . Since the magnetic field predominates, the gyro-radius is closely given by  $r_g = 0.4/\omega = 0.0016$ , with gyro-period  $T = 2\pi/\omega \approx 0.02513$ . We needed  $\Delta t = 0.1975$ , approximately eight times the gyro-period, to closely match the 13 first-order oscillations of Parker and Birdsall's[4] original Fig.1. No such large first-order oscillations are seen in EB2B's trajectory. Fig.7(a) is primarily used to verify the  $\mathbf{E} \times \mathbf{B}$  drift velocity  $v_d = 1/\omega = 0.004\hat{\mathbf{y}}$ , this drift can again be removed so that EB1A's and EB1B's error can be easily shown in Fig.7(b). Since the first-order gyro-radius  $R_g \approx r_g\theta/2$  at large  $\theta$  and its off-set is also  $r_g\theta/2$ , its maximum deviation from the true gyro-center is  $\pm r_g\theta = \pm 0.079$ . This is the top most and bottom most horizontal lines in Fig.7 (b). By contrast, EB2B only oscillates near zero within the true gyro-radius  $\pm 0.0016$ .

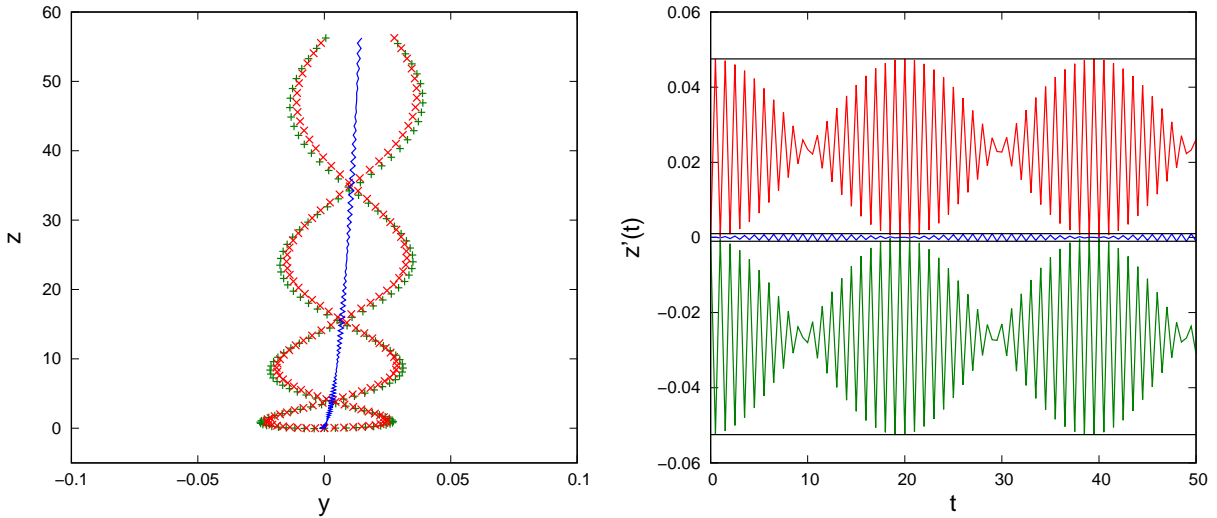


FIG. 8. (color online) **Left** (a): Polarization drift calculation using EB1A (green), EB1B (red) and EB2B (blue) at  $\Delta t = 0.5$ . **Right** (b): The oscillation of  $z'(t) = z(t) - 0.01t^2$  for measuring gyro-diameters of all three Boris solvers.

In Fig.8(a) we use the same three solvers to reproduce Parker and Birdsall's[4] Fig.4 on the polarization drift with  $\mathbf{E} = (-2t)\hat{\mathbf{y}}$ ,  $\mathbf{B} = 100\hat{\mathbf{x}}$ ,  $\mathbf{r}_0 = \mathbf{0}$  and  $\mathbf{v}_0 = 0.1\hat{\mathbf{z}}$ . Again the large first-order gyro-radius oscillations are absent from EB2B's trajectory. Since the gyro-center off-sets are in the direction of  $\mathbf{v}_0 = 0.1\hat{\mathbf{z}}$ , they are not visible along the  $y$ -coordinate. The  $\mathbf{E} \times \mathbf{B}$  velocity drift here is  $\mathbf{v}_d = (2t)/B \hat{\mathbf{z}}$ . Removing the resulting coordinate drift gives  $z'(t) = z(t) - 0.01t^2$  which is plotted in Fig.8(b). The top and the bottom lines are 0.04751 and  $-0.052467$  from zero, giving *different* gyro-diameters to EB1B and EB1A respectively. (This is due to the subtle ways in which EB1A and EB1B integrates

the time-dependent electric force. For EB1A, the first time steps evaluates the electric force at  $t = 0$ , while EB1B evaluate it at  $t = \Delta t$ . The resulting different  $v_{\perp}$  then produces a slightly different  $r_g$ .) However, their average is correctly  $0.04999 = r_g \theta$ . Again, EB2B's gyro-diameter showed no such  $\Delta t$ -dependence and is correctly bracketed by  $\pm r_g = \pm 0.001$  around zero.

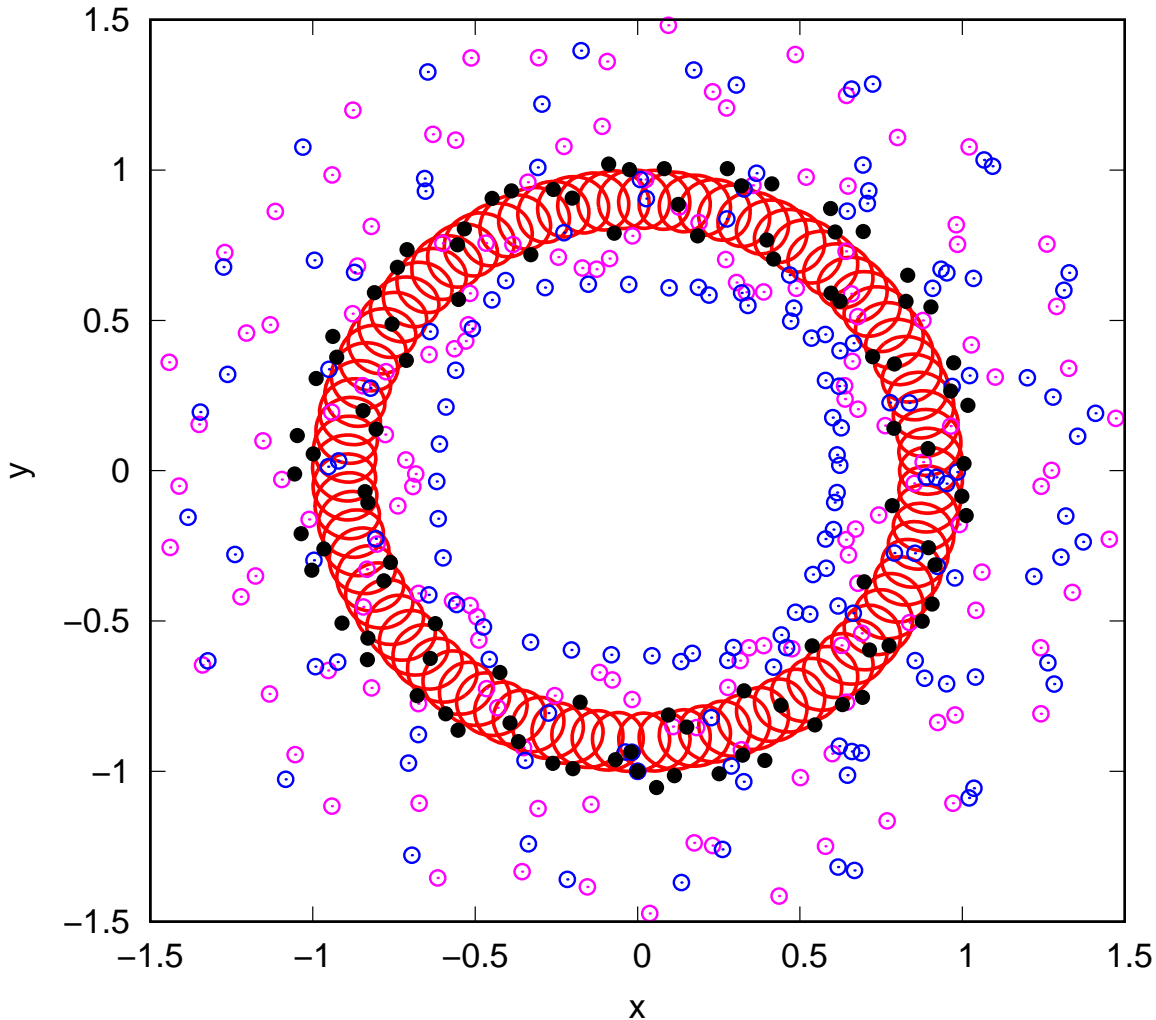


FIG. 9. (color online) Open purple and blue circles are trajectories of first-order Boris solvers EB1A and EB1B. Solid black circles are trajectory points of the second-order Boris solver EB2B. All with  $\Delta t = 2.1\pi$ . They are to be compared with the solid red cycloid produced by EM2B at  $\Delta t = \pi/10$ . See text for details.

For a more modern comparison, with combined  $\nabla \mathbf{B}$  and  $\mathbf{E} \times \mathbf{B}$  drifts, the following 2D

field configuration from Ref.9,

$$\mathbf{B} = r\hat{\mathbf{z}} \quad \mathbf{a} = \frac{10^{-1}}{r^3}(x\hat{\mathbf{x}} + y\hat{\mathbf{y}}) \quad (5.16)$$

with  $r = \sqrt{x^2 + y^2}$ , is also tested. For  $\mathbf{r}_0 = (0, -1)$  and  $\mathbf{v}_0 = (0.1, 0.01)$ , the motion is a super-circle of gyro-circles with gyro-period  $T = 2\pi$ . The trajectory computed with EM2B at  $\Delta t = T/20$  is shown as solid red line in Fig.9. Trajectory points using EB1A, EB1B and EB2B at  $\Delta t = 2.1\pi > T$  are plotted without their distracting connecting lines. The trajectory of EB2B remains close to the exact solution while those of EB1A and EB1B are widely scattered. All non-Boris integrators, such as EM2B, are unbounded at such a large  $\Delta t$ .

## VI. CONCLUSIONS AND FUTURE DIRECTIONS

In this work, we have derived various Boris solvers on the basis of the Lie operator method, the same method used to derive symplectic integrators. The advantage of this method is that it reveals trajectory errors which are the root basis for Boris solvers not obvious from finite-difference schemes. The glaring off-set error of the gyro-center, as well as that of the gyro-radius, can be used to easily identify first-order leap-frog Boris solvers in historical calculations and current discussions.

The distinction between first and second-order Boris solver is how the *position* is updated, not just before or after the velocity update, but before *and* after. Neglecting this seemingly trifle distinction seriously degrades the Boris solver to first-order with large errors.

Historically, Buneman's  $\mathbf{E} \times \mathbf{B}$  method of incorporating the electric field was thought to be inferior[3, 4] to Boris's  $\mathbf{E}$ ,  $\mathbf{B}$  splitting scheme. By deriving  $\mathbf{E}$  and  $\mathbf{B}$  algorithms from the Lie operator method, this work showed that Boris's scheme is equivalent to Buneman's method, but only for the original Boris angle.

By repeating some historical calculations, this work showed the second-order Boris solver EB2B, can be use for large  $\Delta t$  calculations with far greater accuracy than previously thought. It is the only algorithm currently known to be stable at  $\Delta t$  greater than the local gyro-period for nonuniform fields. The obvious future direction is to devise beyond second-order, more accurate Boris-like integrators which are simultaneously stable at large time steps.

**Declaration of competing interest**

The authors declare that they have no known competing financial interests or personal relationships that could have appeared to influence the work reported in this paper.

### Data availability

The data that supports the findings of this study are available from the corresponding author upon reasonable request.

### Funding:

This research did not receive any specific grant from funding agencies in the public, commercial, or not-for-profit sectors.

## Appendix A: Two exact magnetic field solvers

Appendix A of Ref.15 has shown that two second-order algorithms for a constant magnetic field can be exactly on the gyro-circle if the updating steps in (4.2) are modified to

$$\begin{aligned}
 \mathbf{v}_1 &= \mathbf{v}_B(\mathbf{r}_0, \mathbf{v}_0, \Delta t/2) \\
 \mathbf{r}_1 &= \mathbf{r}_0 + \Delta t \left[ \mathbf{v}_1 + g(\theta) \hat{\mathbf{B}} \times (\hat{\mathbf{B}} \times \mathbf{v}_1) \right] \\
 \mathbf{v}_2 &= \mathbf{v}_B(\mathbf{r}_1, \mathbf{v}_1, \Delta t/2)
 \end{aligned} \tag{A1}$$

and those in (4.3) are modified to

$$\begin{aligned}
 \mathbf{r}_1 &= \mathbf{r}_0 + \frac{1}{2} \Delta t \left[ \mathbf{v}_0 + h(\theta) \hat{\mathbf{B}} \times (\hat{\mathbf{B}} \times \mathbf{v}_0) \right] \\
 \mathbf{v}_1 &= \mathbf{v}_B(\mathbf{r}_1, \mathbf{v}_0, \Delta t) \\
 \mathbf{r}_1 &= \mathbf{r}_1 + \frac{1}{2} \Delta t \left[ \mathbf{v}_1 + h(\theta) \hat{\mathbf{B}} \times (\hat{\mathbf{B}} \times \mathbf{v}_1) \right]
 \end{aligned} \tag{A2}$$

with

$$g(\theta) = 1 - \frac{\sin(\theta/2)}{(\theta/2)} \tag{A3}$$

$$h(\theta) = 1 - \frac{\tan(\theta/2)}{(\theta/2)}. \tag{A4}$$

The essence of the Boris solver is to decouple the rotation angles in (A3) and (A4) from  $\theta$  to  $\theta_C$  and  $\theta_B$  such that  $\sin(\theta_C/2) = \theta/2$  and  $\tan(\theta_B/2) = \theta/2$ , forcing  $g(\theta) = 0 = h(\theta)$  and (A1) and (A2) back to the form (4.2) and (4.3), yielding solvers C2A and B2B.

In Appendix B of Ref.15 the same two conditions  $g(\theta) = 0 = h(\theta)$  also yield exact trajectories in a constant electric and magnetic field.

- 
- [1] O. Buneman, “Time-Reversible Difference Procedures”, *J. Comput. Phys.* 1, 517 (1967).
- [2] J. Boris, in *Proceedings of the Fourth Conference on Numerical Simulation of Plasmas*, (Naval Research Laboratory, Washington DC, 1970), p. 3.
- [3] C. Birdsall and A. Langdon, *Plasma Physics Via Computer Simulation* (McGraw-Hill, Inc., New York, 1985), p. 356.
- [4] S.E. Parker and C.K. Birdsall, “Numerical error in electron orbits with large  $\omega_{ce}\Delta t$ ”, *J. Comput. Phys.* 97 (1991) 91–102.
- [5] H.X. Vu, J.U. Brackbill, “Accurate numerical solution of charged particle motion in a magnetic field”, *J. Comput. Phys.* 116(2) (1995) 384–387.
- [6] J. L. Vay, “Simulation of beams or plasmas crossing at relativistic velocity”, *Phys. Plasmas* 15, 056701 (2008); <https://doi.org/10.1063/1.2837054>
- [7] H. Qin, S. X. Zhang, J. Y. Xiao, J. Liu, Y. J. Sun, and W. M. Tang, “Why is Boris algorithm so good?” *Phys. Plasmas* 20, 084503 (2013).
- [8] P. H. Stoltz, J. R. Cary, G. Penn, and J. Wurtele, “Efficiency of a Boris like integration scheme with spatial stepping,” *Phys. Rev. Spec. Top. Accel. Beams* 5, 094001 (2002).
- [9] Y. He, Y. J. Sun, J. Liu, and H. Qin, “Volume-preserving algorithms for charged particle dynamics,” *J. Comput. Phys.* 281, 135 (2015)
- [10] Seiji Zenitani<sup>1</sup> and Takayuki Umeda “On the Boris solver in particle-in-cell simulation” *Phys. Plasmas* 25, 112110 (2018)
- [11] B. Ripperda , F. Bacchini , J. Teunissen , C. Xia , O. Porth , L. Sironi , G. Lapenta , and R. Keppens “A Comprehensive Comparison of Relativistic Particle Integrators”, *Astrophys. J. Suppl. Series*, 235:21, (2018), <https://doi.org/10.3847/1538-4365/aab114>.
- [12] L. F. Ricketsona and L.Chacónb, “An energy-conserving and asymptotic-preserving charged-particle orbit implicit time integrator for arbitrary electromagnetic fields” *J. Comput. Phys.* 418 (2020) 109639.
- [13] Siu A. Chin, “A fundamental derivation of two Boris solvers and the Ge-Marsden theorem”, [arXiv:2106.04068v2](https://arxiv.org/abs/2106.04068v2).
- [14] Christian Knapp, Alexander Kendl, Antti Koskela, and Alexander Ostermann “Splitting methods for time integration of trajectories in combined electric and magnetic fields” *Phys.*

- Rev. E 92, 063310 (2015)
- [15] Siu A. Chin, “Symplectic and energy-conserving algorithms for solving magnetic field trajectories”, Phys. Rev. E 77, 066401 (2008).
- [16] A. Deprit, “Canonical transformations depending on a small parameter,” Celestial Mech. Dyn. Astron. 1, 12–39 (1969).
- [17] A. J. Dragt and J. M. Finn, “Lie series and invariant functions for analytic symplectic maps”, J. Math. Phys. 17, 2215-2224 (1976).
- [18] H. Yoshida, “Recent progress in the theory and application of symplectic integrators”, Celest. Mech. Dyn. Astron. 56, 27-43 (1993).
- [19] Sergio Blanes and Fernando Casas *A Concise Introduction to Geometric Numerical Integration*, Chapman and Hall/CRC, 2016
- [20] Siu A. Chin, “Structure of numerical algorithms and advanced mechanics”, Am. J. Phys. 88, 883 (2020); doi: 10.1119/10.0001616